Supporting Information

Construction of logic gate computation and visual test paper for methyl paraoxon assay based on a fluorescent europium–organic framework

Nan Li,[a,b] Yanyan Yu,[a] Yuanyuan Zhou,[a] Kexin Xu,[a], Yunshan Zhou,*[a] Lijuan Zhang,*[a] Yuxu Zhong*[b]

[a]State Key Laboratory of Chemical Resource Engineering, College of Chemistry, Beijing University of Chemical Technology, Beijing 100029, P. R. China.

[b]Toxicology and Medical Countermeasures, Beijing Institute of Pharmacology and Toxicology, Beijing 100850, P. R. China.

* Corresponding author: Yunshan Zhou
E-mail: zhouys@mail.buct.edu.cn;
* Corresponding author: Lijuan Zhang
E-mail: ljzhang@mail.buct.edu.cn;
* Corresponding author: Yuxu Zhong
E-mail: yuxuzhong2008@aliyun.com

Reagents and chemicals

Europium nitrate hexahydrate ($Eu(NO_3)_3 \cdot 6H_2O$) and 1,4-naphthalenic acid (1,4-H_2NDC) were purchased from Bide Pharmatech Ltd. Cetyltrimethylammonium bromide (CTAB) and triethylamine (TEA) were acquired from Macklin Co., Ltd. N,N-Dimethylformamide (DMF) was obtained from Damao (Tianjin) Chemical Reagent Factory Co., Ltd. Methyl paraoxon (DMNP) was purchased from J&K Scientific Ltd. Polyacrylonitrile was purchased from Tianjin Xi'ensi Co., Ltd standard M_w 150,000 g mol. All the other chemical reagents were analytical-grade and used without further purification.

Characterization

Fourier-transform infrared (FTIR) spectra were acquired over the range of 4000–400 cm^{-1} on a Nicolet FTIR-170SX Fourier transform infrared spectrometer after preparing a KBr pellet of the material. Powder X-ray diffraction (PXRD) was conducted on a SHIMADZU XRD-600 diffractometer with Cu Kα radiation (λ = 0.15405 nm) at a scan rate of 10°/min over the 2θ range of 5–50°. Thermogravimetric analysis (TGA) was performed on a NETZSCH STA 449 C thermal analyzer at a heating rate of 10°C/min under air atmosphere. Scanning electron microscope (SEM) images and energy-dispersive spectroscopy (EDS) mappings were obtained by using a Zeiss 500 high revolution field emission instrument. Particle size distribution of the MOF was estimated using a Malvern ZEN 3600 Zetasizer Nano System with the DLS method. Photoluminescence excitation spectrum and emission spectrum were recorded at room temperature using an Edinburgh Instruments FLS1000 spectrometer. The room-temperature luminescence decay curves were also collected by utilizing a single-photon-counting spectrometer from FLS1000 spectrometer equipped with a 327 nm nanosecond pulse lamp as the excitation source. The absolute photoluminescence quantum yields were measured using an Edinburgh Instruments' FLS1000 fluorescence spectrophotometer attached with an integrating sphere through an absolute method (λ_{ex} = 327 nm). The Commission International de I'Eclairage (CIE) color coordinates were defined and calculated according to the internal CIE standards. N_2 adsorption–desorption isotherms and pore structure of the MOF were measured at liquid nitrogen temperature (77 K) with a Micromeritics ASAP 2010 gas sorption analyzer. The fluorescence response of the MOF to DMNP was recorded using a SpectraMax iD3 microplate reader. The fluorescence emission spectra were acquired over the range of 550–750 nm with excitation at 327 nm. X-ray photoelectron spectroscopy (XPS) was carried out using a Thermo Fisher ESCALAB 250Xi X-ray photoelectron spectroscope. The Ultraviolet–visible spectra were recorded on a Shimazu UV2500 instrument. Fibrous strips were prepared by an electrospinning machine (E05-001) purchased from Foshan Lepton Precision Measurement and Control Technology Co., Ltd. Density functional theory (DFT) was applied to calculate the singlet energy level and the triplet energy level of ligand 1,4-H_2NDC, the highest occupied molecular orbital energies and the lowest unoccupied molecular orbital energies of both 1,4-H_2NDC and DMNP.

Single-crystal structure determination

Single-crystal X-ray diffraction data were collected by a Bruker APEX2 X-Diffraction instrument in ω-scan mode using Mo Kα radiation (λ = 0.71073Å). The structure was solved directly, and anisotropic refinement was performed using the full-matrix least-squares method by the SHELX 97 software package.[1] The positions of non-hydrogen atoms were determined by successive difference Fourier syntheses. The final refinement of non-hydrogen atoms in F was performed by full-matrix least-squares with anisotropic thermal parameters.[2, 3] The crystallographic data and structural parameters of Eu-NDC are provided in Table S1, and selected bond distances and angles of Eu-NDC are provided in Table S2.

Table S1 Crystallography data of Eu-NDC

Formula	$C_{48}H_{46}Eu_2N_4O_{16}\cdot 1.5C_3H_7NO$
λ (Å)	0.71073
T (K)	99.7(2) K
Crystal system	triclinic
Space group	*P*-1
Volume	2618.0(3) $Å^3$
Density	2.176 mg/m^3
Unit cell dimensions	a = 11.3797(5) Å
	b = 11.4685(8) Å
	c = 23.1474(17) Å
	α = 78.490(6)°
	β = 87.392(6)°
	γ = 62.339(6)°
Z	2
ρ_{calc} (mg/mm^3)	1.711
μ (mm^{-1})	2.453
F (000)	1352
Index ranges	$-15 \le h \le 15, -15 \le k \le 15, -29 \le l \le 29$
2θ range for date collection	5.97 to 58.676°
Crystal size	0.15 × 0.11 × 0.04 mm^3
Data/restraints/parameters	12031/165/780
Reflection collected	21429
Independent reflections	12031[R(int) = 0.0291, R_{sigma} = 0.0501
Goodness-of-fit on F^2	1.051
Final R indexes [$I \ge 2\sigma$ (I)]	R_1 = 0.0312, wR_2 = 0.0648
R indexes [all data]	R_1 = 0.0397, wR_2 = 0.0688
Largest diff. peak/hole/ ($e\cdot Å^{-3}$)	1.20/–0.98
CCDC deposition number	2219729

Table S2 Selected bond distances [Å] and angles [°] for Eu-NDC

Eu-NDC			
Bond	Length	Bond	Length
Eu(1)-O(2)	2.383(2)	Eu(2)-O(1)	2.534(2)
Eu(1)-O(3)#1	2.485(2)	Eu(2)-O(2)	2.618(2)
Eu(1)-O(4)#1	2.454(2)	Eu(2)-O(5)	2.388(2)
Eu(1)-O(6)	2.399(2)	Eu(2)-O(7)#2	2.400(2)
Eu(1)-O(8)#2	2.370(2)	Eu(2)-O(9)	2.497(2)

Eu(1)-O(11)#3	2.501(2)	Eu(2)-O(10)	2.422(2)
Eu(1)-O(12)#3	2.633(2)	Eu(2)-O(12)#3	2.377(2)
Eu(1)-O(13)	2.439(2)	Eu(2)-O(15)	2.423(2)
Eu(1)-O(14)	2.437(2)	Eu(2)-O(16)	2.453(2)
Moiety	Angle	Moiety	Angle
O(2)-Eu(1)-O(3)#1	79.47(8)	O(1)-Eu(1)-O(2)	50.46(7)
O(6)-Eu(1)-O(12)#2	71.02(7)	O(9)-Eu(2)-O(2)	139.87(7)
O(6)-Eu(1)-O(13)	143.38(8)	O(10)-Eu(2)-O(1)	149.11(7)
O(6)-Eu(1)-O(14)	76.01(8)	O(10)-Eu(2)-O(2)	144.45(8)
O(8)#3-Eu(1)-O(12)#2	69.40(7)	O(12)#2-Eu(2)-O(5)	74.41(8)
O(8)#3-Eu(1)-O(13)	71.66(8)	O(12)#2-Eu(2)-O(7)#3	75.97(8)
O(8)#3-Eu(1)-O(14)	143.54(8)	O(12)#2-Eu(2)-O(9)	77.40(8)
O(11)#2-Eu(1)-O(12)#2	50.45(7)	O(12)#2-Eu(2)-O(10)	83.10(8)
O(13)-Eu(1)-O(3)#1	108.60(8)	O(12)#2-Eu(2)-O(15)	142.52(8)
O(13)-Eu(1)-O(4)#1	74.50(8)	O(12)#2-Eu(2)-O(16)	142.59(8
O(14)-Eu(1)-O(11)#2	73.42(9)	O(16)-Eu(2)-O(1)	72.78(7)
O(14)-Eu(1)-O(12)#2	118.09(8)	O(16)-Eu(2)-O(2)	107.84(7)
O(14)-Eu(1)-O(13)	72.33(8)	O(16)-Eu(2)-O(9)	112.18(8)

Symmetry codes: #1: 2-x, -y, 2-z; #2: -1+x, +y, +z; #3: 2-x, -y, 1-z.

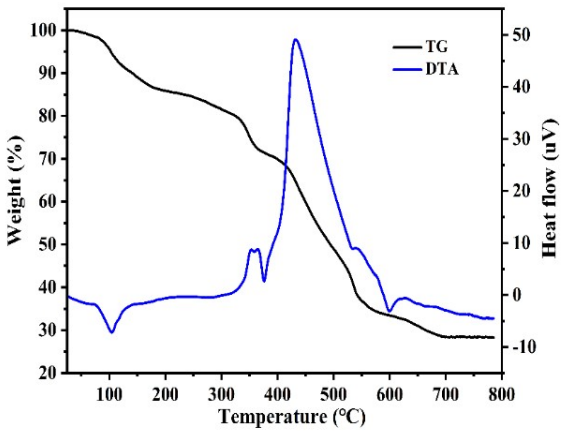

Fig. S1 TG-DTA curves of Eu-NDC.

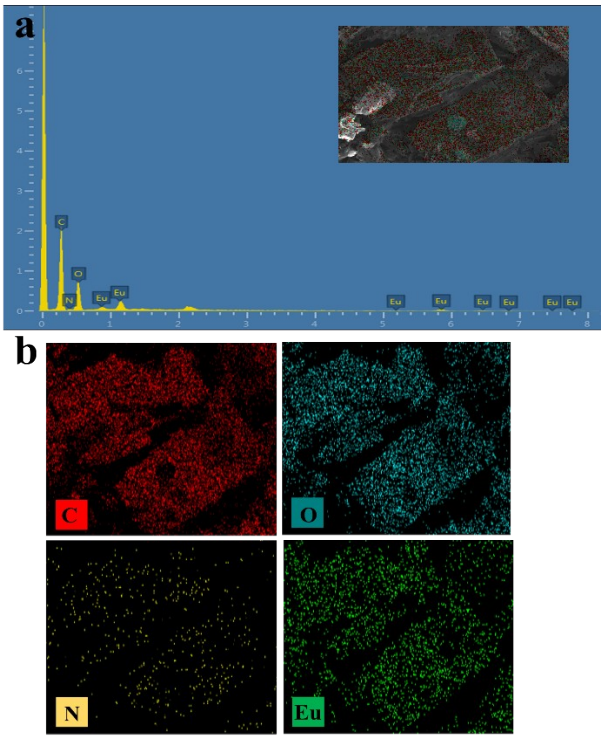

Fig. S2 The EDS spectrum (a) and EDS mapping (b) of Eu-NDC.

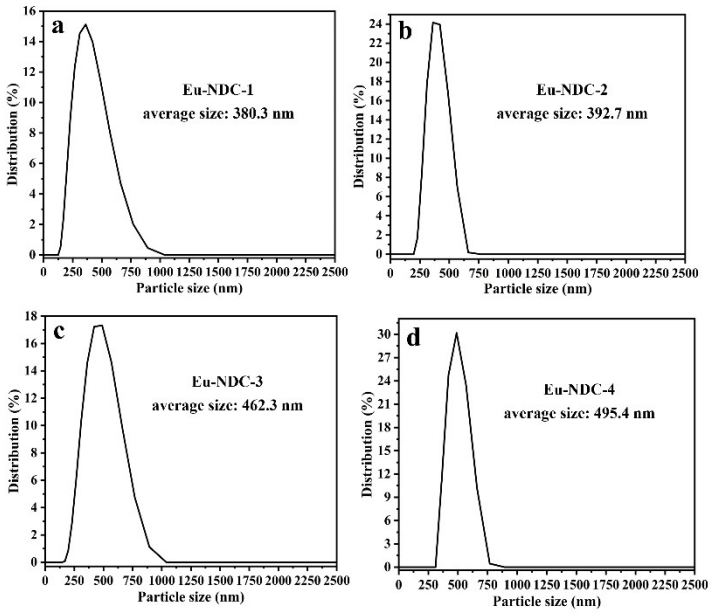

Fig. S3 Particle size distribution of Eu-NDC-1/2/3/4 (a/b/c/d) in ethanol.

Table S3. Fitting parameters for fluorescence decay curves.

	A	B_1	τ_1	B_2	τ_2
Eu-NDC	1.265	164.423	0.281	954.243	1.388
Eu-NDC-1	7.962	775.891	0.226	1545.559	1.883
Eu-NDC-2	6.193	650.891	0.227	1720.485	1.912
Eu-NDC-3	4.877	208.979	0.329	1863.157	1.978
Eu-NDC-4	7.601	864.330	0.177	1647.324	1.899

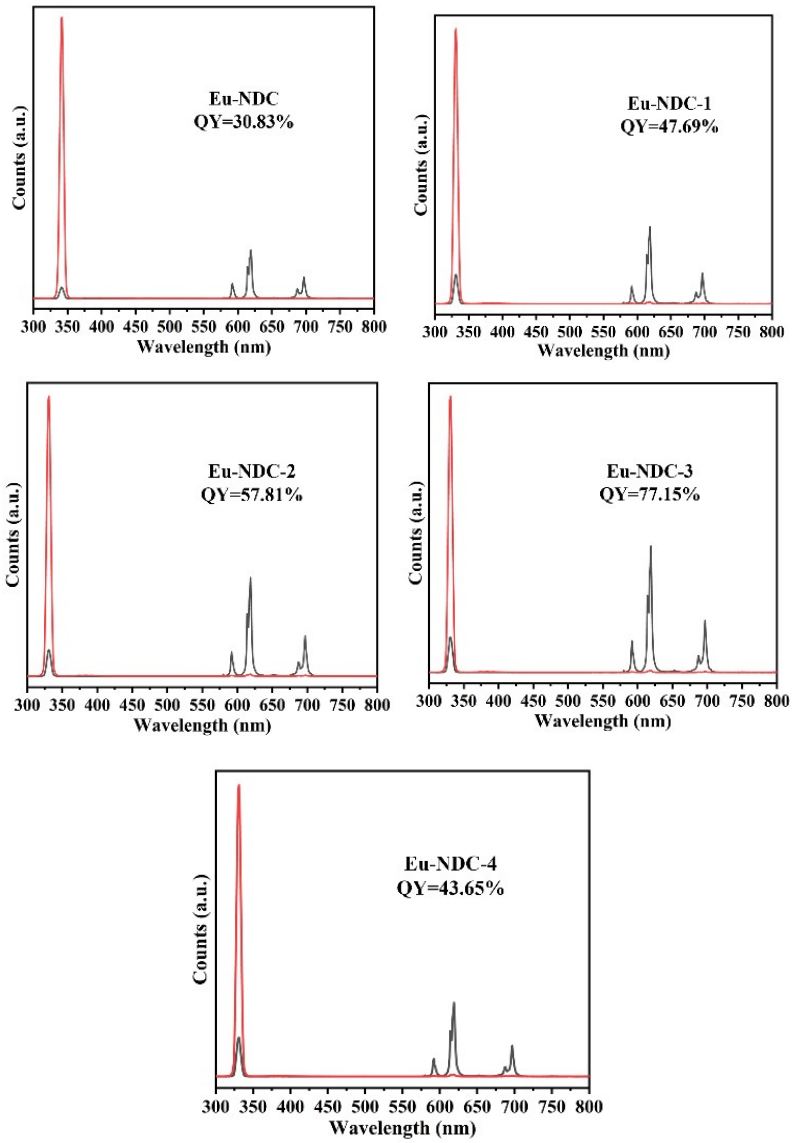

Fig. S4 The absolute solid-state quantum yields (QY) of Eu-NDC and Eu-NDC-1/2/3/4.

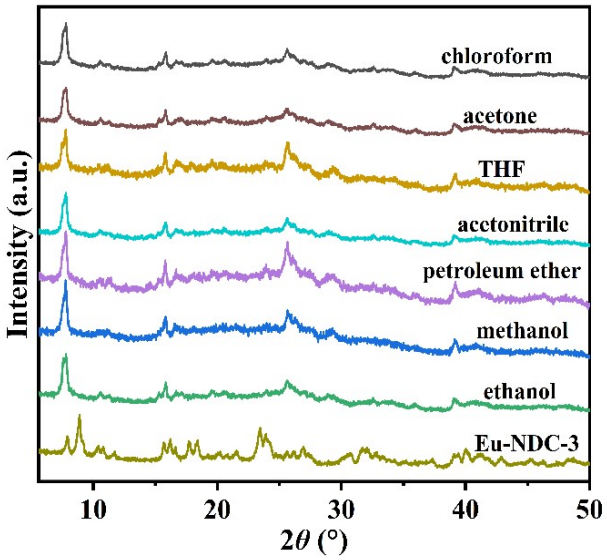

Fig. S5 The PXRD patterns of Eu-NDC-3 immersed in multiple organic solvents for 2 days.

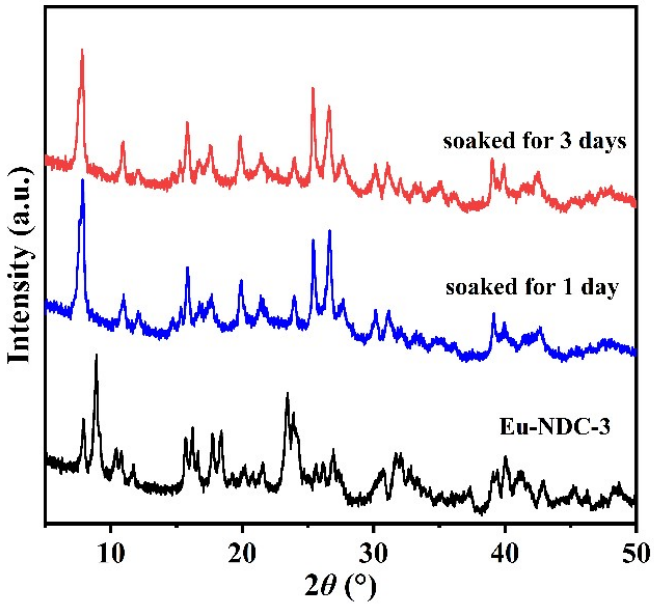

Fig. S6 The PXRD patterns of Eu-NDC-3 immersed in water for 24 h and 72h.

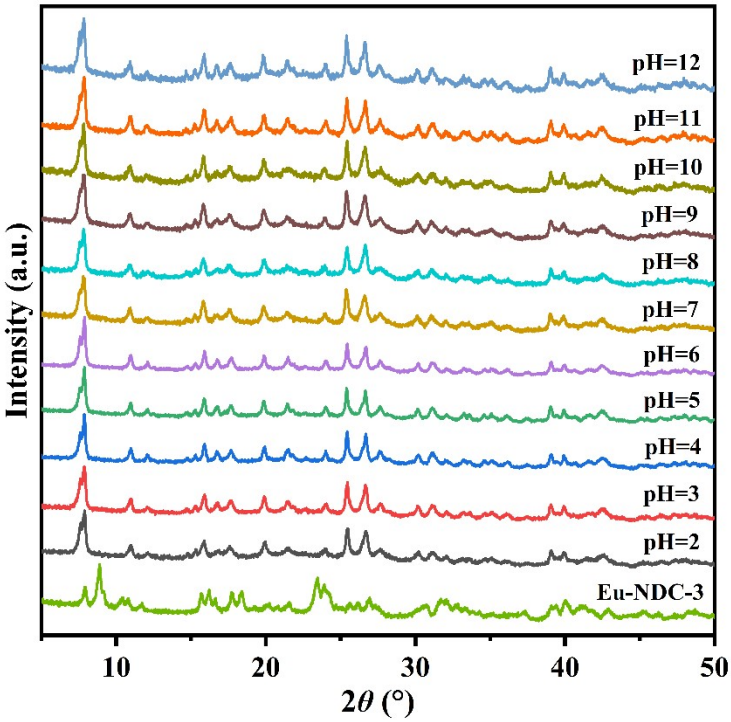

Fig. S7 The stability of Eu-NDC-3 by immersing in HCl or NaOH solutions with pH =1-14 for 24h.

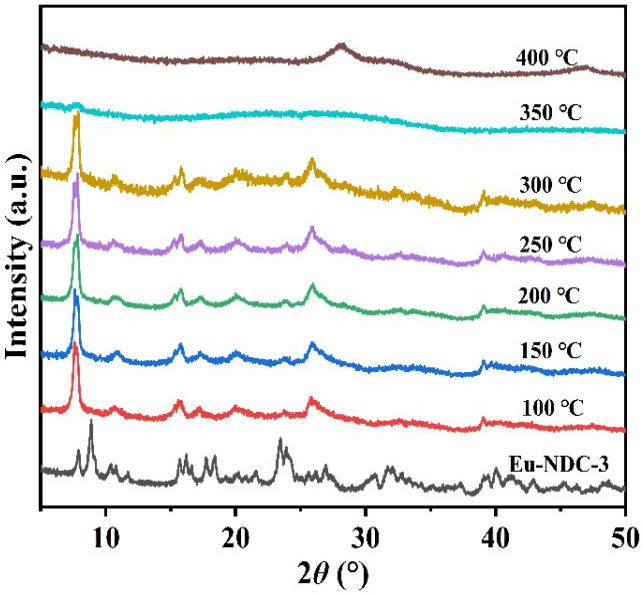

Fig. S8 The PXRD patterns of Eu-NDC-3 treated under different temperatures.

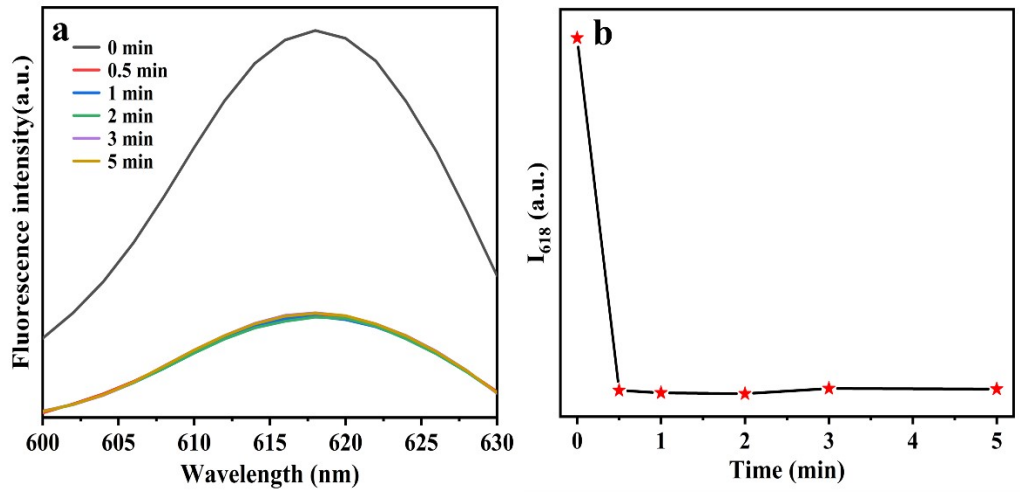

Fig. S9 Time dependent fluorescence spectra (λex = 327 nm) of Eu-NDC (0.68 mg/mL) upon the addition of DMNP (22.62 μM) in ethanol (a). The fluorescence intensity at 618 nm as a function of time (b).

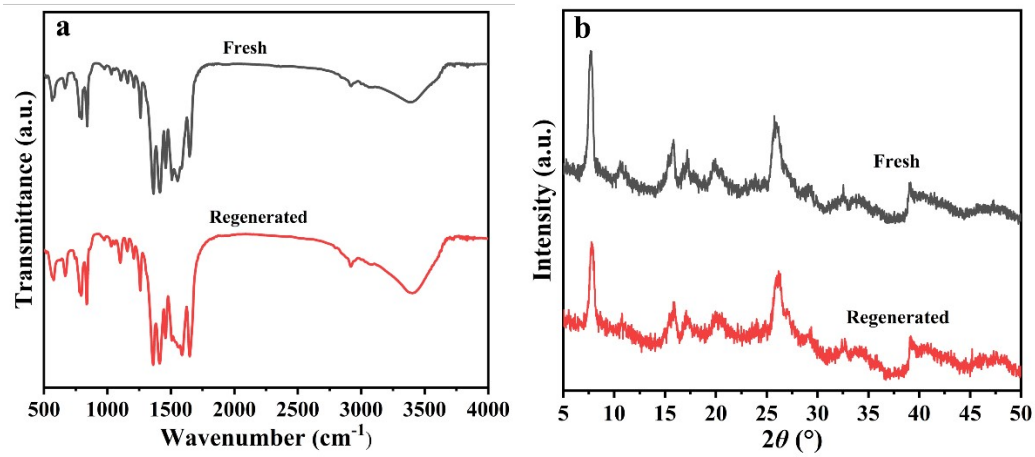

Fig. S10 FT-IR (a), and PXRD (b) of Eu-NDC-3 (Fresh) and DMNP-treated Eu-NDC-3 (Regenerated).

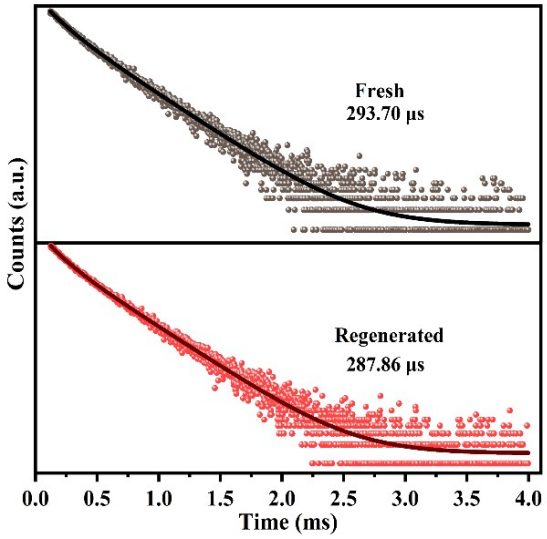

Fig. S11 The fluorescence decay curves of Eu-NDC-3 (Fresh) and DMNP-treated Eu-NDC-3 (Regenerated).

Table S4. Fitting parameters for fluorescence decay curves.

	A	B_1	τ_1	B_2	τ_2
Eu-NDC-3	1.189	1623.435	0.138	1766.057	0.350
DMNP-treated Eu-NDC-3	1.446	2734.004	0.128	2936.338	0.343

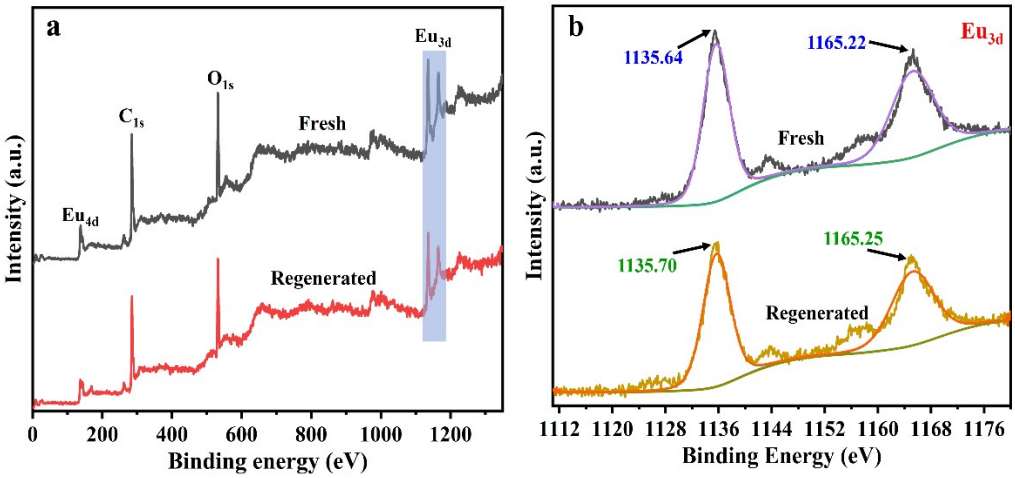

Fig. S12 The XPS survey spectrum with a rectangular bar in gray highlighting the Eu_{3d} peaks (a) and the Eu_{3d} high-resolution spectrum of Eu-NDC-3 (Fresh) and DMNP-treated Eu-NDC-3 (Regenerated).

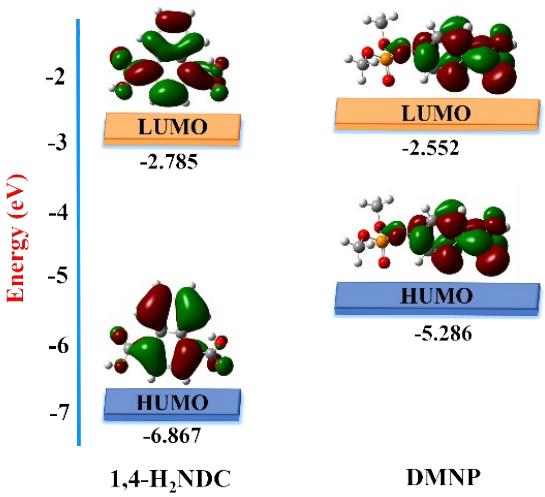

Fig. S13 The HOMO and LUMO energy levels of 1,4-H_2NDC and DMNP.

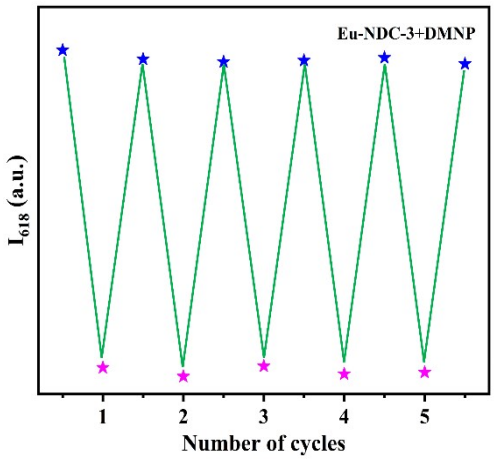

Fig. S14 I_{618} of Eu-NDC-3 during five continuous quenching by DMNP and regenerating cycles. The blue and pink stars respectively represented the I_{618} of Eu-NDC-3 suspension (0.68 mg/mL) before and after adding DMNP (22.62 μM).

Table S5. The truth table of the logic gates.

Gate 1	Input 1		Output 1
	C > 2.83 μM		Light 1
	0		1
	1		0
Gate 2	Input 2		Output 2
	C > 22.62 μM		Light 2
	1		0
	0		1
Gate 3	Input 3		Output 3
	Output 1	Output 2	Light 3
	1	0	0
	0	0	1
	0	1	0

Table S6 Comparison of various reported sensing systems for DMNP

Method	Material	Mechanism	Linear range (μM)	LOD (nM)	Response time (min)	Recyclability	logic-gate system	Visual test paper
Fluorometry	GQDs[4]	DMNP inhibited the AChE activity	0.4–4.05	7.78×10^{2}	35	No	No	No
	$Ru(bpy)_3^{2+}$ and ThT@ZnCPs[5]		4.1×10^{-3}–1.22	9.3×10^{-1}	60	No	No	Yes
	NCDs[6]	Hydrolysis of DMNP by OPH	2.4–73.8	3.4×10^{2}	30	No	No	No
	Mn:ZnS QDs[7]		0.19–0.95	2.0×10^{1}	10	No	No	No
	CQDs/QDs-peptide[8]	Hydrolysis of DMNP by metalloenzymes mimics	0.12–100	3.5×10^{1}	12	Yes	No	No
	TPE-Peptide[9]	DMNP induced TPE attached onto the peptide to aggregate and emit light	1–100	6.0×10^{2}	15	No	No	No
	CTAB-CdTe QDs[10]	Electron transfer between CTAB-CdTe QDs and DMNP	4.5×10^{-3}–40.5	4.8×10^{1}	5	No	No	No
	Per-6-amino-β-cyclodextrin: Eu complex[11]	DMNP competently binds to Eu^{3+} by substituting coordination water	unknown	1.0×10^{1}	10	No	No	No
Electrochemistry	Hal-MWCNTs[12]	Redox reaction of the nitro group of DMNP	0.5–11	3.4×10^{1}	1	Yes	No	No
	N-MAL-CDs[13]	DMNP inhibited the AChE activity	3.8×10^{-9}–3.8×10^{-4}	1.4×10^{-6}	14	No	No	No
	TiO_2@DA@S/H/E nanoenzyme[14]	Hydrolysis of DMNP by TiO_2@DA@S/H/E nanoenzyme	0.5–100	2.0×10^{2}	5	Yes	No	No
Colorimetry	Nanoceria[15]	DMNP inhibited the AChE activity	0–2.8	7.4×10^{1}	50	No	No	Yes
	$NaBH_4$[16]	Hydrolysis of DMNP by $NaBH_4$	0.11–11.50	2.0×10^{2}	15	No	No	No
SERS	Au-coated surface[17]	Raman signals of DMNP	unknow	$< 10^{5}$	unknow	Yes	No	No
Fluorometry	**Eu-NDC-3**	Competitive absorption	0-5.7	8.5×10^{1}	<0.5	Yes	Yes	Yes

References

1. G. M. Sheldrick, *SHELXL-97. Program for the Refinement of Crystal Structures*, 1997.
2. G. M. Sheldrick, *SHELXS-97, Program for the Solution of Crystal Structures*, 1997.
3. G. Sheldrick, G. M. Sheldrick and G. M. Sheldrick, *SHELXTL V5.1: Software Reference Manual*, 1997.
4. C. Sahub, T. Tuntulani, T. Nhujak and B. Tomapatanaget, *Sens. Actuat. B: Chem.*, 2018, **258**, 88-97.
5. Y. Li, Z. Huang, B. Liu, Z.-Z. Huang, H. Yang and H. Tan, *Biosens. Bioelectron.*, 2023, **220**, 114890.
6. W. Song, H.-J. Zhang, Y.-H. Liu, C.-L. Ren and H.-L. Chen, *Chin. Chem. Lett.*, 2017, **28**, 1675-1680.
7. F. Zhang, Y. Liu, P. Ma, S. Tao, Y. Sun, X. Wang and D. Song, *Talanta*, 2019, **204**, 13-19.
8. Y. Yang, X. Lei, B. Liu, H. Liu, J. Chen, G. Fang, J. Liu and S. Wang, *Sens. Actuat. B: Chem.*, 2023, **377**, 133031-133042.
9. J. Wang, J. Zhang, J. Wang, G. Fang, J. Liu and S. Wang, *J. Hazard. Mater.*, 2020, **389**, 122074-122081.
10. N. Fahimi-Kashani and M. R. Hormozi-Nezhad, *Sens. Actuat. B: Chem.*, 2020, **322**, 128580-128588.
11. K. Kanagaraj, A. Affrose, S. Sivakolunthu and K. Pitchumani, *Biosens. Bioelectron.*, 2012, **35**, 452-455.
12. H. Zhao, H. Ma, X. Li, B. Liu, R. Liu and S. Komarneni, *Appl. Clay Sci.*, 2021, **200**, 105907-105917.
13. J. Xu, C. Yu, T. Feng, M. Liu, F. Li, Y. Wang and J. Xu, *Nanoscale*, 2018, **10**, 19390-19398.
14. L. Qiu, P. Lv, C. Zhao, X. Feng, G. Fang, J. Liu and S. Wang, *Sens. Actuat. B: Chem.*, 2019, **286**, 386-393.
15. S. Nouanthavong, D. Nacapricha, C. S. Henry and Y. Sameenoi, *Analyst*, 2016, **141**, 1837-1846.
16. M.-P. N. Bui and A. Abbas, *Sens. Actuat. B: Chem.*, 2015, **207**, 370-374.
17. A. Das, N. Gupta, A. K. Agrawal and A. Dhawan, *RSC Adv.*, 2022, **12**, 9645-9652.